Hydrogen chemisorption on polycyclic aromatic hydrocarbons via tunnelling

Goumans, T.P.M.

Monthly Notices
of the
ROYAL ASTRONOMICAL SOCIETY

Mon. Not. R. Astron. Soc. **415,** 3129–3134 (2011) doi:10.1111/j.1365-2966.2011.18924.x

Hydrogen chemisorption on polycyclic aromatic hydrocarbons via tunnelling

T. P. M. Goumans★

Gorlaeus Laboratories, Leiden Institute of Chemistry, Leiden University, PO Box 9502, 2300 RA Leiden, the Netherlands

Accepted 2011 April 15. Received 2011 April 14; in original form 2011 February 10

ABSTRACT

The chemisorption of hydrogen atoms on polycyclic aromatic hydrocarbons (PAHs) is studied at low temperatures via quantum mechanical tunnelling through reaction barriers. PAHs are ubiquitous in the interstellar medium and may exist in various charge states as well as hydrogenation states. PAHs have been suggested to catalyze H_2 formation in photon-dominated regions via chemisorbed hydrogen atoms. Hydrogenated PAHs are also implicated by the relative strengths of the infrared bands in protoplanetary nebulae, reflection nebulae and H II regions. The activation barrier for the chemisorption of hydrogen atoms to graphite is prohibitively high (∼5000 K) at low to moderate temperatures for this reaction to occur classically. On PAHs, however, edge sites are more flexible and can accommodate the incoming hydrogen atom more easily, resulting in a lower barrier. Combined with a further rate enhancement via tunnelling, hydrogen chemisorption on PAH edges may become feasible in various regions in the interstellar medium. We present harmonic quantum transition state theory calculations, which incorporate tunnelling, on pyrene as a model PAH system. Indeed the relatively low (∼2000 K) classical activation barriers for hydrogen atom chemisorption on edge sites combined with strong tunnelling give rise to non-negligible rates of the order of 10^{-16}–10^{-18} cm^3 site^{-1} s^{-1} at temperatures as low as 40 K, with a large kinetic isotope effect $k_H/k_D \approx 64$, characteristic for tunnelling. At this temperature, chemisorption on the core of a PAH is orders of magnitude slower, $\sim 10^{-22.5}$ cm^3 site^{-1} s^{-1} even for the lightest H isotope. The addition of H atoms to PAH edge sites via tunnelling could be efficient enough to contribute H-PAH formation, although other processes may be more important.

Key words: astrochemistry – molecular processes – ISM: atoms – ISM: molecules.

1 INTRODUCTION

Polycyclic aromatic hydrocarbons (PAHs) are observed throughout the interstellar medium (ISM) through their mid-infrared (mid-IR) features (Tielens 2008). In particular, the larger PAHs (>50 C atoms) are resilient enough to escape the degradation by the harsh interstellar radiation field (Le Page, Snow & Bierbaum 2003; Tielens 2008). PAHs are profuse in the ISM, with fractional abundances locking up 5 per cent of the elemental C in photon-dominated regions (PDRs) (Tielens 2008) or 15–20 per cent in the diffuse ISM (Dwek et al. 1997; Zubko, Dwek & Arendt 2004). A recent study suggests that if more correct oscillator strengths are used, PAH abundances may be a factor of 2–5 higher (Tan et al. 2011).

Aromatic C–H stretches centred at 3.3 μm dominate the interstellar mid-IR, while aromatic C–D stretches at 4.4 μm are difficult to positively identify (Peeters et al. 2004), which indicates that deuterium is not likely to be locked up in PAHs. Hydrogenated PAHs (H_n-PAHs), however, have been implied by aliphatic C–H features in the 3.4- and 6.2-μm regions (Bernstein, Sandford & Allamandola 1996; Wagner & et al. 2000; Beegle, Wdowiak & Harrison 2001; Song et al. 2006).

Through correlations between H_2 and PAH abundances, it has also been suggested that PAHs are involved in the catalytic formation of H_2 in PDRs via H chemisorption to yield H_n-PAHs (Habart et al. 2004). In PDRs, temperatures are too high for H_2 formation to occur via the Langmuir–Hinshelwood association of physisorbed H atoms on graphitic grains. Jonkheid et al. (2006) have also suggested that H_2 is formed on PAHs in evolved discs. Furthermore, H-PAHs are suggested to be key intermediates for CO formation via $C^+ \rightarrow CH^+ \rightarrow\rightarrow\rightarrow$ CO in protoplanetary discs (Jonkheid et al. 2007).

Previously, we have calculated that through efficient tunnelling, indeed the addition rate for H to benzene is non-negligible at moderate to low temperatures (Goumans & Kästner 2010). Here we extend this study to H addition to a more realistic model of the PAH

★E-mail: t.goumans@chem.leidenuniv.nl

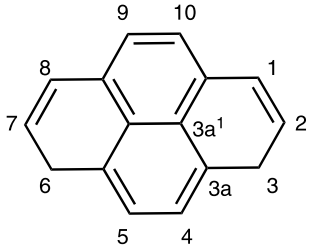

Figure 1. Numbering of the C atoms of pyrene. All peripheral C atoms 1–10 are C–H groups.

pyrene ($C_{16}H_{10}$, Fig. 1) via quantum tunnelling. Rauls & Hornekaer (2008) have calculated that the classical barrier for the addition to the peripheral C atoms of coronene ($C_{24}H_{10}$) is much reduced compared to the addition at a central C atom, which could facilitate the formation of H_n-PAHs.

2 METHODOLOGY

2.1 Harmonic quantum transition state theory

Harmonic quantum transition state theory (HQTST) is a reformulation of the instanton or Imaginary F theory which uses discretized Feynman paths to optimize the tunnelling path in all dimensions, while treating modes perpendicular to the tunnelling path as quantum harmonic oscillators. The HQTST methodology has been described in great detail before (Arnaldsson 2007; Andersson et al. 2009; Rommel, Goumans & Kästner 2011); therefore, we just briefly summarize the method and its sensitivities here.

Within the HQTST approximation, the most probable tunnelling path at a given temperature is fully optimized in all N dimensions without any restriction on the geometry of the path as opposed to other semiclassical methods such as small-curvature tunnelling (close to the minimum energy path) or large-curvature tunnelling (a straight-line tunnelling path). In the HQTST, the optimal tunnelling path is represented by the Feynman path integral with the highest statistical weight, that is, the saddle point on the minimum action path (MAP) from the reactant to product. Mathematically, the MAP saddle point is equivalent to the unstable orbit on the upside-down potential (instanton), but these unstable orbits are very difficult to locate for any potential beyond one dimension. Conversely, in the HQTST approach, the MAP saddle point search is effectively done by discretizing the closed Feynman path in P images and searching for a first-order saddle point on the $N \times P$ dimensional action surface. Once the optimal tunnelling path, or quantum transition state (qTS), is found, the reaction rate is calculated as

$$k = \frac{1}{\Phi_{\rm rel}} \frac{1}{Q_{\rm R,vib}} \sqrt{\frac{S_0}{2\pi h}} \frac{1}{\Delta\tau \left| \prod_j' \lambda_j \right|} {\rm e}^{-\frac{S_{\rm ins}}{\hbar}},$$

where $\Phi_{\rm rel}$ is the relative translational partition per unit volume,

$$\Phi_{\rm rel} = \left(\frac{2\pi\mu k_{\rm B} T}{h^2} \right)^{3/2},$$

with μ the reduced mass, $k_{\rm B}$ the Boltzmann constant and h the Planck constant. S_0 is twice the action of the qTS due to the imaginary time kinetic energy:

$$S_0 = \frac{\mu P k_{\rm B} T}{\hbar} \sum_j^P |q_{\,{\rm mod}\,(j,P)+1} - q_j|^2,$$

with P the number of images and q_j the coordinates of image j. $Q_{\rm R,vib}$ is the vibrational partition of the reactant, which is resolved as a discretized Feynman path with P images and $\Delta\tau$ is the imaginary time-step $\hbar/(k_{\rm B}TP)$. $|\Pi_j' \lambda_j|$ is the vibrational partition function of the qTS, where the zero modes (one extra zero mode comes from the permutation of the images) are omitted and the instable mode is inverted.

$$S_{\rm ins}/\hbar = \frac{1}{k_{\rm B}T} \sum_{j=1}^{P} \left[\frac{k_{\rm sp}(T)}{2} |q_{\,{\rm mod}\,(j,P)+1} - q_j|^2 + \frac{V(q_j)}{P} \right]$$

is the instanton action, with $k_{\rm sp}$ the temperature-dependant spring constant, $k_{\rm sp} = \mu P (\frac{k_{\rm B}T}{\hbar})^2$, and $V(q_j)$ the potential energy of image q_j. Comparing the HQTST with classical TST, the factor $S_{\rm ins}/\hbar$ operates as an effective Boltzmann factor $E_{\rm eff}/k_{\rm B}T$ in an Arrhenius-type expression, where the tunnelling effect is naturally incorporated in the Euclidean action $S_{\rm ins}$, which serves to lower the apparent activation energy to $E_{\rm eff}$. We do not include rotational partition functions in the rate calculations (can be treated classically even at 40 K), since the moments of inertia of a large PAH do not differ from its H addition TS, cancelling the contribution from rotation.

For exact analytical potentials, the HQTST approach is usually in excellent agreement at low T with analytical solutions or accurate quantum dynamics (QD) methods (Arnaldsson 2007), while other semiclassical tunnelling approaches perform better at higher T. Sometimes the harmonic approximation to the modes perpendicular to the tunnelling path is inaccurate and an anharmonic treatment is necessary for quantitative agreement between the HQTST and QD (Andersson et al. 2009). Here we use a direct dynamics approach where energies and first and second derivatives of the entire system are calculated on the fly from an external quantum chemistry code. Since hundreds of thousands of force calls and thousands of Hessians had to be calculated for this study, we had to resort to computationally feasible yet accurate methods such as density functional theory (DFT). This may introduce extra errors (apart from the semiclassical and harmonic approximations) in the reaction rates because the chosen computational approach may be inaccurate.

2.2 Choice of the density functional approach

In a previous study on the H + benzene (the simplest 'PAH') reaction, we tested several DFT approaches against a high-level *ab initio* benchmark calculation at the CCSD(T) level (Goumans & Kästner 2010). In this study, we found that the MPWB1K functional with a 6-31G*(*) basis set was the best approach, because with this approach:

(1) the calculated barrier and the reaction rates are in good agreement with the CCSD(T) calculation at the complete basis set (CBS) limit and with experiments in the high-T regime; and

(2) the energies along the long tunnelling path at 20 K are in good agreement with accurate CCSD(T)-F12/cc-VTZ calculations.

The other functionals we tested (PW91, PBE, B3LYP) have been previously used in the literature to study H + graphite/PAH reactions (Jeloaica & Sidis 1999; Sha, Jackson & Lemoine 2002; Hornekaer et al. 2006b; Rougeau, Teillet-Billy & Sidis 2006). PW91 and PBE are standard generalized gradient approximation (GGA) functionals and B3LYP is a hybrid GGA with a low percentage of exact exchange, and these appear to underestimate the height of the H + benzene reaction significantly (∼1200 K), as has been often observed for various other activation barriers (Zhao & Truhlar 2005).

With the ultrafine integration grid employed in our study, the effect of the basis set on the calculated barrier is found to be small.

Table 1. Calculated electronic barriers $E^{\ddagger}$ (in K) for the addition of H to naphthalene at the 9-position with various functionals and basis sets.

Basis set	MPWB1K	B3LYP	PBE	PW91
6-31G*(*)	5240	4110	3680	3510
6-311+G**	4860	3810	3300	3140
aug-cc-pVTZ	4990	3890	3390	3260

Table 2. Calculated ZPEs, electronic barriers $E^{\ddagger}$, vibrational adiabatic barriers $V*_{\rm ad}$ and $T_{\rm c}$ for the H or D addition to pyrene at various sites (Fig. 1). All values are in units of K.

Atom	H	D	H	D	H	D
Site	1	1	4	4	$3a^1$	$3a^1$
ZPE	434	251	456	268	645	374
$E^{\ddagger}$	1451	1451	1612	1612	4483	4483
$V*_{\rm ad}$	1884	1702	2068	1880	5128	4857
$T_{\rm c}$	185.1	141.8	189.7	145.4	270.7	211.7

For all functionals, the H + benzene barrier is slightly increased if the large aug-cc-pVTZ basis set is used, ranging from 117 K (PBE) to 227 K (B3LYP). With this large basis set, the B3LYP result is still 900 K lower than the benchmark CCSD(T)/CBS calculation, while the PBE and PW91 barriers are lower still. The MPWB1K barrier becomes slightly worse (higher) with this larger basis set than with the 6-31G*(*) basis set, but is still in better agreement than the other functionals tested.

For larger PAHs, the only system we could study at a reasonably high level [CCSD(T)-F12/cc-VTZ//MP2/cc-VTZ] is the symmetric addition of a H atom to a central atom of naphthalene (the 9-position). At this level, the electronic activation barrier is 5940 K, while with all tested DFT approaches (Table 1) the barriers are lower. As was the case for H + benzene reactions, the DFT barriers are of the order MPWB1K << B3LYP < PBE < PW91, albeit that in this case a larger basis set reduces the barrier (see Table 1). The activation barrier for H addition to a central naphthalene carbon is slightly higher than for the addition to a core site on pyrene (see Table 2).

Since the 6-31G*(*) basis set is computationally more efficient than larger basis sets, and the MPWB1K functional with this basis set agrees best with the two benchmark calculations for H addition to aromatic systems, we chose to use the MPWB1K/6-31G*(*) electronic structure method for our direct dynamics HQTST calculations.

2.3 Convergence of the HQTST reaction rates

The qTSs were optimized with NwChem (Bylaska 2007) and its second derivatives calculated with gaussian03 (Frisch 2004). The forces of the qTS are converged to at least 10^{-3} eV Å^{-1}, because even tighter convergence criteria lead to enormous numbers of force calls ($>10^5$) at low T. The convergence of the rates is checked with respect to an increase in the number of images P, and also with respect to the instanton length S_0 and the Hessian eigenmodes: if a second negative eigenvalue appears for the qTS Hessian, then this is indicative of too few images. With the current convergence criteria, the HQTST reaction rates could fluctuate somewhat, especially at lower temperatures (e.g. for $T/T_{\rm c} < 0.2$, $\log k$ could fluctuate by ± 0.4); therefore, we only report reaction rates down to 40 K. The fluctuation in the rates appeared to be due to the vibrational prefactor of the qTS, which is sensitive to the exact position of the images for long tunnelling paths (large C–H distances) at low temperature. A recent algorithm with an adaptive discretization scheme for the Feynman path may reduce some of this noise and allow for less number of images to resolve the Feyman path (Rommel & Kästner, private communication), but at large atomic distances DFT Hessians and thereby the qTS vibrational partition function is still anticipated to be noisy, which makes it difficult to converge HQTST bimolecular reaction rates with the direct dynamics DFT at very low T.

The qTS becomes more delocalized with decreasing temperature and consequently more images are necessary to properly resolve the closed Feynman path and therefore rate coefficients need to be converged with respect to increasing the number of images used to discretize the Feynman path. The qTS is optimized at a number of temperatures, starting just below the crossover temperature $T_{\rm c} = h\omega* /2\pi k_{\rm B}$, with $\omega*$ the imaginary frequency of the instable mode, where tunnelling starts to dominate, down to 40 K. At 40 K, 98 images are needed to converge the HQTST rates, and we could not obtain converged rates below this temperature, because of the high dimensionality of the qTS and the extended delocalization of the qTS, leading to numerical inaccuracies with this functional due to the noise in the DFT energies, forces and harmonic frequencies.

We fit our HQTST results for the rate coefficient per addition site on the PAHs between $T_{\rm c}$ and 40 K with the modified Arrhenius expression:

$$k = \alpha \left(\frac{T}{300}\right)^{\beta} {\rm e}^{-\frac{\gamma}{T}}\ {\rm cm^3\ site^{-1}\ s^{-1}}. \quad (1)$$

Good (0.991 for H addition at the core $3a^1$ position) to excellent (>0.997) correlation coefficients are obtained for these fits. The classical TST rate data with a simple Wigner tunnelling correction (Wigner 1938) at temperatures between 2000 K and $T_{\rm c}$ are relevant, for instance, in shock regions and hot cores, and can be extremely well fitted (correlation coefficients >0.999) to separate modified Arrhenius expressions.

3 RESULTS

The vibrational adiabatic barrier for a reaction consists of the electronic contribution, the potential energy of the TS minus the reactant state, and a zero-point energy (ZPE) contribution. In Table 2, the ZPEs, electronic barriers and vibrational adiabatic barriers are reported for the reaction of H and D atoms with pyrene at the edge positions 1 and 4 and at the core position $3a^1$ (Fig. 1). Rauls & Hornekaer (2008) have found that the H addition to aromatic C–H groups at the edge of PAHs is much more favourable than the addition to core C atoms, which is also what we find here, although the absolute barrier heights differ because of the different functionals used. The enhanced reactivity of edge atoms is caused by the increased flexibility of the rehybridizing C atom. This is demonstrated by the tunnelling paths at 40 K for edge (4) and core ($3a^1$) adsorption depicted in Fig. 2. The puckering (0.15 Å at the end-point of the tunnelling path) of the central C atom for the core addition can be clearly seen as the C atoms participate in the tunnelling motion at 40 K. Conversely, for the H addition to an edge C–H side, C atoms do not participate strongly in the tunnelling motion, thus disrupting the aromatic system to a lesser extent. In general, the optimal tunnelling path can deviate from the minimum energy path (MEP), more strongly so at lower T where the tunnelling path is longer. Because the tunnelling probability depends strongly on the distance

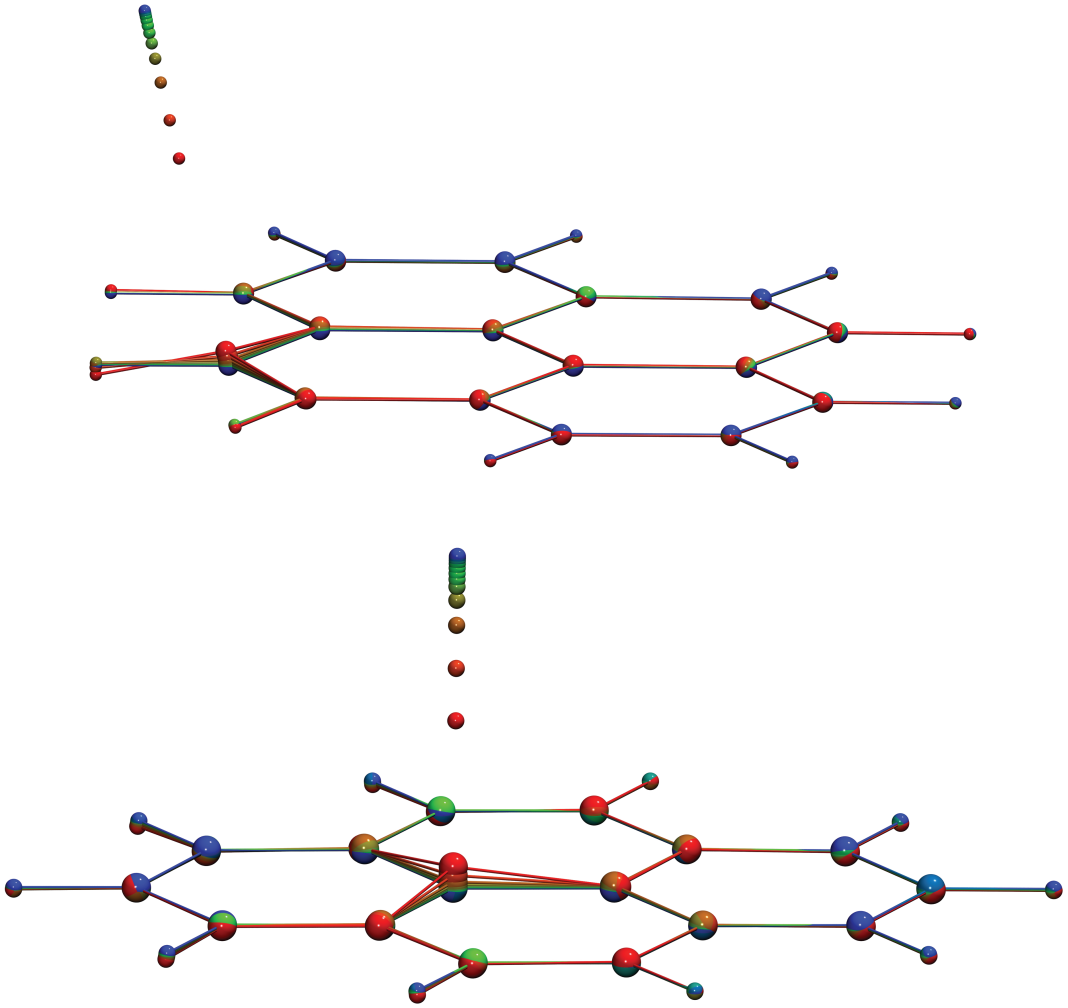

Figure 2. The optimal tunnelling paths, or qTSs, for the H addition to pyrene at the 4 position (top) and the $3a^1$ position (bottom) at 40 K. Every fourth image of the 98 images of the Feynman path is shown, colour-coded from blue (reactant side) to red (product side).

tunnelled, a shorter path may be favoured even though it is higher in energy, an effect known as corner-cutting. For all H additions considered here, the tunnelling path at 40 K lies very close to the MEP.

For pyrene, the vibrational adiabatic barrier for H addition at the 2-position, where the accommodating C–H is flanked by two other C–H groups, is much higher (2950 K) than at either of the other two edge positions. The 1 and 4 positions of pyrene are model sites for the addition to edge C–H sites on larger PAHs, while the $3a^1$ position mimics core PAH sites as well as graphitic sites. The calculated classical activation barriers for the H addition to core and edge sites are comparable for pyrene ($C_{16}H_{10}$) and the larger PAH coronene ($C_{24}H_{12}$). Likewise, the core and edge addition barriers are expected to be similar for the larger PAHs (>50 C atoms) that survive in the ISM.

The high temperatures (2000–2200 K) used experimentally (Zecho et al. 2002; Hornekaer et al. 2006a) to stick H or D atoms to the graphite (0001) surface give rise to high reaction rates ($10^{-11.5}$ cm^3 s^{-1}) with our calculated barriers, allowing sufficiently fast H chemisorption under these conditions. In contrast, the calculated activation barriers would give negligible H addition rates with the classical TST at 40 K to the core (10^{-66} cm^3 site^{-1} s^{-1}) or edge positions 1 and 4 (10^{-30} or 10^{-32} cm^3 site^{-1} s^{-1}) of pyrene. However, at these temperatures, the reactivity is tunnelling-dominated and when tunnelling is included with HQTST, these classical rates are enhanced by 44, 14 and 16 orders of magnitude, that is, the tunnelling transmission coefficients are 10^{44}, 10^{14} and 10^{16}, respectively. In Fig. 3, we have plotted the classical rates for the H addition to the 1, 4 and $3a^1$ sites on pyrene, the calculated HQTST data for H and D additions, and the fits to these data. The modified Arrhenius parameters are summarized in Table 3.

Especially in the tunnelling regime, the phenomenological modified Arrhenius parameters cannot be used outside the fitted temperatures. For instance, the large negative γ-values would lead to sharply increasing rates for decreasing temperatures below 40 K. As can be seen in Fig. 3, the fit for the H addition to the PAH core below T_c (the worst fit) already incorrectly predicts a very slight increase in the rate when lowering the temperature from 50 to 40 K.

Since at 40 K there is already efficient tunnelling leading to near-temperature-independent rates, we suggest using the (averaged) data at 40 K also at temperatures below 40 K: $10^{-22.5}$ cm^3 s^{-1} for the H addition to a PAH core or graphitic site and $10^{-16.9}$ cm^3 s^{-1} for the H addition to an edge PAH site and $10^{-18.7}$ cm^3 s^{-1} for the D addition to an edge PAH site. PAH edges may be deuterated but because the reaction occurs via tunnelling at 40 K, the reaction rate per edge site is 64 times slower than H addition. We did not

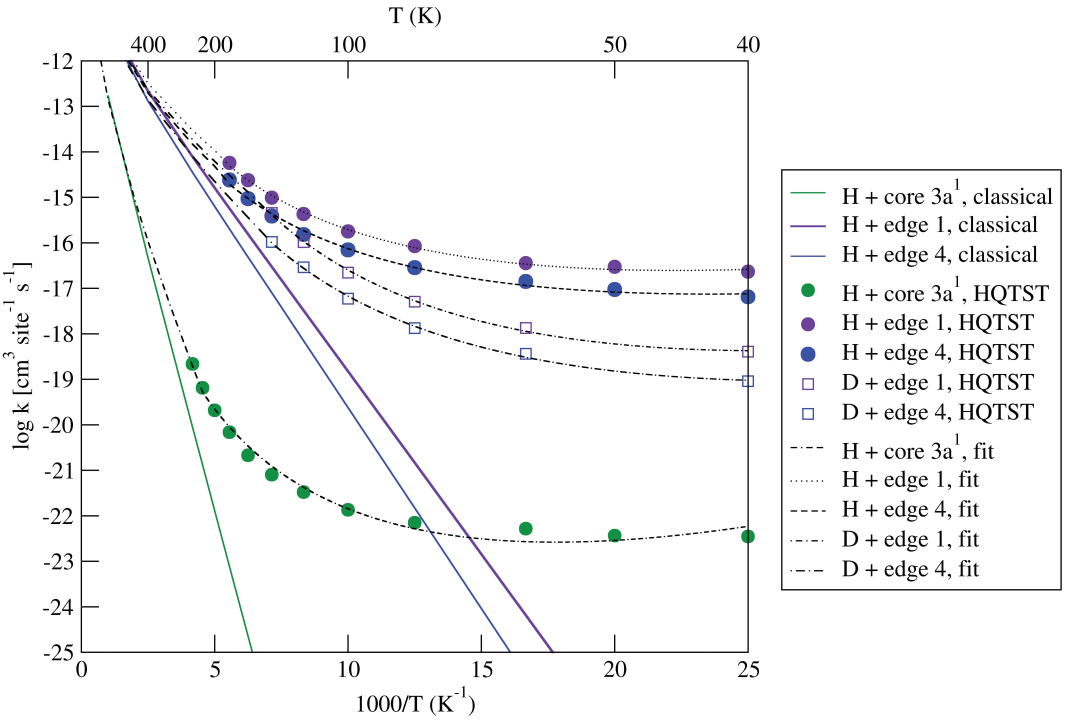

Figure 3. Log of rate coefficients (cm^3 site^{-1} s^{-1}) for the H (closed symbols) and D (open symbols) addition to core and edge pyrene sites (Fig. 1). Full lines: classical TST, data points: HQTST, and broken lines: modified Arrhenius equation fits.

Table 3. Modified Arrhenius parameters for 2000 K–T_c (see Table 2), $\alpha(>T_c)$, $\beta(>T_c)$ and $\gamma(>T_c)$, and for T_c–40 K, $\alpha(\leq T_c)$, $\beta(\leq T_c)$ and $\gamma(\leq T_c)$, for the addition of H and D to pyrene sites (see Fig. 1). α is in units of cm^3 site^{-1} s^{-1}, β is dimensionless and γ is in units of K.

Atom	H	D	H	D	H
Site	1	1	4	4	3a^1
$\alpha(>T_c)$	1.091×10^{-12}	1.167×10^{-12}	8.642×10^{-13}	1.255×10^{-12}	4.457×10^{-14}
$\beta(>T_c)$	2.200	2.039	2.263	1.966	3.272
$\gamma(>T_c)$	746.3	882.6	854.1	1106	2785
$\alpha(\leq T_c)$	4.275×10^{-14}	1.628×10^{-13}	1.848×10^{-14}	3.337×10^{-14}	1.021×10^{-19}
$\beta(\leq T_c)$	8.283	12.40	8.171	11.61	12.26
$\gamma(\leq T_c)$	−371.7	−485.6	−346.7	−425.1	−689.4

calculate the D addition to core PAH sites; however, a similar or larger isotope effect is expected as was calculated for the edge sites, which makes the deuteration of PAH cores and graphite very slow below 300 K.

4 DISCUSSION

We calculated reaction rate coefficients including tunnelling for the H and D additions to model PAH sites. The quantum tunnelling effect makes the reaction rates non-negligible at low temperatures despite sizeable classical activation barriers. Owing to a more favourable barrier, the addition to edge sites is preferred over the core addition at all temperatures. Therefore, peripherally, hydrogenated neutral H_n-PAHs, which according to Wagner et al. (2000) are responsible for the 3.4-μm feature, may be formed in the ISM via the tunnelling addition of H atoms.

The calculated HQTST reaction rate for the H addition to a PAH edge site is $\sim 10^{-16.9}$ cm^3 s^{-1} at 40 K. Assuming a fractional abundance of $7 \times 10^{-5} \times n_H$ for C atoms in PAHs (Dwek et al. 1997) of which 20 per cent are edge C–H sites, the formation rate of H-PAH via tunnelling is $10^{-21.7} \times n_H$ cm^3 s^{-1} at 40 K, $10^{-20.8} \times n_H$ cm^3 s^{-1} at 100 K and $10^{-20} \times n_H$ cm^3 s^{-1} at 140 K. D atom addition at low temperatures is much slower because heavier deuterium tunnels less efficiently than protium. D addition is 64 times slower than H addition at 40 K and 10 times slower at 100 K, but at the onset of tunnelling for D at 140 K the calculated kinetic isotope effect k_H/k_D is only 2.8. The H addition to core sites on PAHs or to graphite is always orders of magnitude lower than the addition to the PAH peripheral C atoms.

H-PAHs are suggested to be essential intermediates for the formation of CO in protoplanetary discs via H-PAH + $C^+ \rightarrow$ PAH + CH^+ and $CH^+ \rightarrow\rightarrow\rightarrow$ CO (Jonkheid et al. 2007). H-PAHs are also implied as catalytic intermediates for the formation of H_2 in PDRs (Habart et al. 2004). Previous calculations suggest that once the first H atom is adsorbed on a carbonaceous surface, subsequent H atoms can adsorb with little or no barrier (Hornekaer et al. 2006; Rougeau et al. 2006; Rauls & Hornekaer 2008; Thrower et al. 2011). Recent experiments have indeed shown that hot D atoms add to coronene, yielding multiply deuterated PAHs (Thrower et al. 2011). The exothermicity for the chemisorption of a second H on a H-PAH or H-graphite may lead to the formation of H_2 via an indirect, 'dimer-mediated' reaction

(Cuppen & Hornekaer 2008), regenerating the PAH. Alternatively, a gas-phase H atom may abstract the chemisorbed H nearly barrierlessly (Sha et al. 2002) either direct (Eley–Rideal mechanism) or after traversing the surface after adsorption (hot atom mechanism). Either way, PAHs may act as a catalyst for H_2 formation via an intermediate state with a chemisorbed H atom at the periphery. For low to moderate temperatures, this chemisorption on PAH edge sites may occur at non-negligible rates ($\sim 10^{-16}$ cm^3 s^{-1}) via quantum tunnelling as suggested by our calculations. Whether or not the H-PAH formation via tunnelling may be an important process under these conditions depends on how it competes with other pathways, such as the addition of H atoms to PAH cations followed by charge neutralization. The calculated tunnelling rates should be incorporated in a full reaction network scheme to assess its potential importance in the ISM.

ACKNOWLEDGMENTS

This work is financially supported by the Netherlands Organisation for Scientific Research (NWO) through a VENI-fellowship (700.58.404). Johannes Kästner is thanked for the direct dynamics implementation of HQTST in ChemShell. Xander Tielens and Ewine van Dishoeck are thanked for useful discussions.

REFERENCES

Andersson S., Nyman G., Arnaldsson A., Manthe U., Jónsson H., 2009, J. Phys. Chem. A, 113, 4468
Arnaldsson A., 2007, PhD thesis, Univ. Washington
Beegle L. W., Wdowiak T. J., Harrison J. G., 2001, Spectrochim. Acta A, 57, 737
Bernstein M. P., Sandford S. A., Allamandola L. J., 1996, ApJ, 472, L127
Bylaska E. J. et al., 2007, NWChem, A Computational Chemistry Package for Parallel Computers, Version 5.1. Pacific Northwest National Laboratory, Richland, WA
Cuppen H. M., Hornekaer L., 2008, J. Chem. Phys., 128, 174707
Dwek E. et al., 1997, ApJ, 475, 565
Frisch M. J. et al., 2004, Gaussian 03, Revision D.01. Gaussian Inc., Wallington, CT
Goumans T. P. M., Kästner J., 2010, Angew. Chem. Int. Ed., 49, 7350
Habart E., Boulanger F., Verstraete L., Walmsley C. M., des Forets G. P., 2004, A&A, 414, 531
Hornekaer L. et al., 2006, Phys. Rev. Lett., 97, 186102
Ioppolo S., Cuppen H. M., Romanzin C., Van Dishoeck E. F., Linnartz H., 2008, ApJ, 686, 1474
Jeloaica L., Sidis V., 1999, Chem. Phys. Lett., 300, 157
Jonkheid B., Kamp I., Augereau J. C., van Dishoeck E. F., 2006, A&A, 453, 163
Jonkheid B., Dullemond C. P., Hogerheigde M. R., van Dishoeck E. F., 2007, A&A, 463, 203
Le Page V., Snow T. P., Bierbaum V. M., 2003, ApJ, 584, 316
Peeters E., Allamandola L. J., Bauschlicher C. W. J., Hudgins D. M., Sandford S. A., Tielens A. G. G. M., 2004, ApJ, 604, 252
Rauls E., Hornekaer L., 2008, ApJ, 679, 531
Rommel J. B., Goumans T. P. M., Kästner J., 2011, J. Chem. Theory Comput., 7, 690
Rougeau N., Teillet-Billy D., Sidis V., 2006, Chem. Phys. Lett., 431, 135
Sha X. W., Jackson B., Lemoine D., 2002, J. Chem. Phys., 116, 7158
Song X. L., Li J. C., Hou H., Wang B. S., 2006, J. Chem. Phys., 125, 094301
Tan X., Bernstein L., Cami J., Salama F., 2011, ApJ, 728, 62
Thrower J. D. et al., 2011, in Joblin C., Tielens A. G. G. M., eds, EAS Publications Ser. Vol. 46, PAHs and the Universe. EDP Sciences, Les Ulis, France
Tielens A. G. G. M., 2008, ARA&A, 46, 289
Wagner D. R., Kim H. S., Saykally R. J., 2000, ApJ, 545, 854
Wigner E., 1938, Trans. Faraday Soc., 34, 29
Zecho T., Guttler A., Sha X. W., Jackson B., Kuppers J., 2002, J. Chem. Phys., 117, 8486
Zhao Y., Truhlar D. G., 2005, J. Phys. Chem. A, 109, 5656
Zubko V., Dwek E., Arendt R. G., 2004, ApJS, 152, 211

This paper has been typeset from a Microsoft Word file prepared by the author.